Fermilab FERMILAB-Pub-01/073-E CDF July 2001

Search for Narrow Diphoton Resonances and for $\gamma\gamma + W/Z$ Signatures in $p\bar{p}$ Collisions at $\sqrt{s} = 1.8$ TeV

May 21, 2001

T. Affolder,[23] H. Akimoto,[45] A. Akopian,[37] M. G. Albrow,[11] P. Amaral,[8] D. Amidei,[25] K. Anikeev,[24] J. Antos,[1] G. Apollinari,[11] T. Arisawa,[45] A. Artikov,[9] T. Asakawa,[43] W. Ashmanskas,[8] F. Azfar,[30] P. Azzi-Bacchetta,[31] N. Bacchetta,[31] H. Bachacou,[23] S. Bailey,[16] P. de Barbaro,[36] A. Barbaro-Galtieri,[23] V. E. Barnes,[35] B. A. Barnett,[19] S. Baroiant,[5] M. Barone,[13]

G. Bauer,[24] F. Bedeschi,[33] S. Belforte,[42] W. H. Bell,[15] G. Bellettini,[33] J. Bellinger,[46] D. Benjamin,[10] J. Bensinger,[4] A. Beretvas,[11] J. P. Berge,[11] J. Berryhill,[8] A. Bhatti,[37] M. Binkley,[11] D. Bisello,[31] M. Bishai,[11] R. E. Blair,[2] C. Blocker,[4] K. Bloom,[25] B. Blumenfeld,[19] S. R. Blusk,[36] A. Bocci,[37] A. Bodek,[36] W. Bokhari,[32] G. Bolla,[35] Y. Bonushkin,[6] D. Bortoletto,[35] J. Boudreau,[34] A. Brandl,[27] S. van den Brink,[19] C. Bromberg,[26] M. Brozovic,[10] E. Brubaker,[23] N. Bruner,[27] E. Buckley-Geer,[11] J. Budagov,[9] H. S. Budd,[36] K. Burkett,[16] G. Busetto,[31] A. Byon-Wagner,[11] K. L. Byrum,[2] S. Cabrera,[10] P. Calafiura,[23] M. Campbell,[25] W. Carithers,[23] J. Carlson,[25] D. Carlsmith,[46] W. Caskey,[5] A. Castro,[3] D. Cauz,[42] A. Cerri,[33] A. W. Chan,[1] P. S. Chang,[1] P. T. Chang,[1] J. Chapman,[25] C. Chen,[32] Y. C. Chen,[1] M. -T. Cheng,[1] M. Chertok,[5] G. Chiarelli,[33] I. Chirikov-Zorin,[9] G. Chlachidze,[9] F. Chlebana,[11] L. Christofek,[18] M. L. Chu,[1] Y. S. Chung,[36] C. I. Ciobanu,[28] A. G. Clark,[14] A. Connolly,[23] J. Conway,[38] M. Cordelli,[13] J. Cranshaw,[40] R. Cropp,[41] R. Culbertson,[11] D. Dagenhart,[44] S. D'Auria,[15] F. DeJongh,[11] S. Dell'Agnello,[13] M. Dell'Orso,[33] L. Demortier,[37] M. Deninno,[3] P. F. Derwent,[11] T. Devlin,[38] J. R. Dittmann,[11] A. Dominguez,[23] S. Donati,[33] J. Done,[39] M. D'Onofrio,[33] T. Dorigo,[16] N. Eddy,[18] K. Einsweiler,[23] J. E. Elias,[11] E. Engels, Jr.,[34] R. Erbacher,[11] D. Errede,[18] S. Errede,[18] Q. Fan,[36] R. G. Feild,[47] J. P. Fernandez,[11] C. Ferretti,[33] R. D. Field,[12] I. Fiori,[3] B. Flaugher,[11] G. W. Foster,[11] M. Franklin,[16] J. Freeman,[11] J. Friedman,[24] H. J. Frisch,[8] Y. Fukui,[22] I. Furic,[24] S. Galeotti,[33] A. Gallas,[(**) 16] M. Gallinaro,[37] T. Gao,[32] M. Garcia-Sciveres,[23] A. F. Garfinkel,[35] P. Gatti,[31] C. Gay,[47] D. W. Gerdes,[25] P. Giannetti,[33] P. Giromini,[13] V. Glagolev,[9] D. Glenzinski,[11] M. Gold,[27] J. Goldstein,[11] I. Gorelov,[27] A. T. Goshaw,[10] Y. Gotra,[34] K. Goulianos,[37]

C. Green,[35] G. Grim,[5] P. Gris,[11] L. Groer,[38] C. Grosso-Pilcher,[8] M. Guenther,[35] G. Guillian,[25] J. Guimaraes da Costa,[16] R. M. Haas,[12] C. Haber,[23] S. R. Hahn,[11] C. Hall,[16] T. Handa,[17] R. Handler,[46] W. Hao,[40] F. Happacher,[13] K. Hara,[43] A. D. Hardman,[35] R. M. Harris,[11] F. Hartmann,[20] K. Hatakeyama,[37] J. Hauser,[6] J. Heinrich,[32] A. Heiss,[20] M. Herndon,[19] C. Hill,[5] K. D. Hoffman,[35] C. Holck,[32] R. Hollebeek,[32] L. Holloway,[18] R. Hughes,[28] J. Huston,[26] J. Huth,[16] H. Ikeda,[43] J. Incandela,[11] G. Introzzi,[33] J. Iwai,[45] Y. Iwata,[17] E. James,[25] M. Jones,[32] U. Joshi,[11] H. Kambara,[14] T. Kamon,[39] T. Kaneko,[43] K. Karr,[44] H. Kasha,[47] Y. Kato,[29] T. A. Keaffaber,[35] K. Kelley,[24] M. Kelly,[25] R. D. Kennedy,[11] R. Kephart,[11] D. Khazins,[10] T. Kikuchi,[43] B. Kilminster,[36] B. J. Kim,[21] D. H. Kim,[21] H. S. Kim,[18] M. J. Kim,[21] S. B. Kim,[21] S. H. Kim,[43] Y. K. Kim,[23] M. Kirby,[10] M. Kirk,[4] L. Kirsch,[4] S. Klimenko,[12] P. Koehn,[28] K. Kondo,[45] J. Konigsberg,[12] A. Korn,[24] A. Korytov,[12] E. Kovacs,[2] J. Kroll,[32] M. Kruse,[10] S. E. Kuhlmann,[2] K. Kurino,[17] T. Kuwabara,[43] A. T. Laasanen,[35] N. Lai,[8] S. Lami,[37] S. Lammel,[11] J. Lancaster,[10] M. Lancaster,[23] R. Lander,[5] A. Lath,[38] G. Latino,[33] T. LeCompte,[2] A. M. Lee IV,[10] K. Lee,[40] S. Leone,[33] J. D. Lewis,[11] M. Lindgren,[6] T. M. Liss,[18] J. B. Liu,[36] Y. C. Liu,[1] D. O. Litvintsev,[11] O. Lobban,[40] N. Lockyer,[32] J. Loken,[30] M. Loreti,[31] D. Lucchesi,[31] P. Lukens,[11] S. Lusin,[46] L. Lyons,[30] J. Lys,[23] R. Madrak,[16] K. Maeshima,[11] P. Maksimovic,[16] L. Malferrari,[3] M. Mangano,[33] M. Mariotti,[31] G. Martignon,[31] A. Martin,[47] J. A. J. Matthews,[27] J. Mayer,[41] P. Mazzanti,[3] K. S. McFarland,[36] P. McIntyre,[39] E. McKigney,[32] M. Menguzzato,[31] A. Menzione,[33] C. Mesropian,[37] A. Meyer,[11] T. Miao,[11] R. Miller,[26] J. S. Miller,[25] H. Minato,[43] S. Miscetti,[13] M. Mishina,[22] G. Mitselmakher,[12] N. Moggi,[3] E. Moore,[27] R. Moore,[25] Y. Morita,[22] T. Moulik,[35] M. Mulhearn,[24] A. Mukherjee,[11] T. Muller,[20] A. Munar,[33] P. Murat,[11] S. Murgia,[26] J. Nachtman,[6] V. Nagaslaev,[40] S. Nahn,[47] H. Nakada,[43] I. Nakano,[17] C. Nelson,[11] T. Nelson,[11] C. Neu,[28] D. Neuberger,[20] C. Newman-Holmes,[11] C.-Y. P. Ngan,[24] H. Niu,[4] L. Nodulman,[2] A. Nomerotski,[12] S. H. Oh,[10] Y. D. Oh,[21] T. Ohmoto,[17] T. Ohsugi,[17] R. Oishi,[43] T. Okusawa,[29] J. Olsen,[46] W. Orejudos,[23] C. Pagliarone,[33] F. Palmonari,[33] R. Paoletti,[33] V. Papadimitriou,[40] D. Partos,[4] J. Patrick,[11] G. Pauletta,[42] M. Paulini,[(*)] [23] C. Paus,[24] L. Pescara,[31] T. J. Phillips,[10] G. Piacentino,[33] K. T. Pitts,[18] A. Pompos,[35] L. Pondrom,[46] G. Pope,[34] M. Popovic,[41] F. Prokoshin,[9] J. Proudfoot,[2] F. Ptohos,[13] O. Pukhov,[9] G. Punzi,[33] A. Rakitine,[24] F. Ratnikov,[38] D. Reher,[23] A. Reichold,[30] A. Ribon,[31] W. Riegler,[16] F. Rimondi,[3] L. Ristori,[33] M. Riveline,[41] W. J. Robertson,[10] A. Robinson,[41] T. Rodrigo,[7] S. Rolli,[44] L. Rosenson,[24] R. Roser,[11] R. Rossin,[31] A. Roy,[35] A. Ruiz,[7] A. Safonov,[12] R. St. Denis,[15] W. K. Sakumoto,[36] D. Saltzberg,[6] C. Sanchez,[28] A. Sansoni,[13] L. Santi,[42] H. Sato,[43] P. Savard,[41] P. Schlabach,[11] E. E. Schmidt,[11] M. P. Schmidt,[47] M. Schmitt,[(**)] [16] L. Scodellaro,[31] A. Scott,[6] A. Scribano,[33] S. Segler,[11] S. Seidel,[27] Y. Seiya,[43] A. Semenov,[9] F. Semeria,[3] T. Shah,[24] M. D. Shapiro,[23] P. F. Shepard,[34] T. Shibayama,[43] M. Shimojima,[43] M. Shochet,[8] A. Sidoti,[31] J. Siegrist,[23] A. Sill,[40] P. Sinervo,[41] P. Singh,[18] A. J. Slaughter,[47] K. Sliwa,[44] C. Smith,[19] F. D. Snider,[11] A. Solodsky,[37] J. Spalding,[11] T. Speer,[14] P. Sphicas,[24] F. Spinella,[33] M. Spiropulu,[16]

L. Spiegel,[11] J. Steele,[46] A. Stefanini,[33] J. Strologas,[18] F. Strumia, [14] D. Stuart,[11] K. Sumorok,[24] T. Suzuki,[43] T. Takano,[29] R. Takashima,[17] K. Takikawa,[43] P. Tamburello,[10] M. Tanaka,[43] B. Tannenbaum,[6]
M. Tecchio,[25] R. Tesarek,[11] P. K. Teng,[1] K. Terashi,[37] S. Tether,[24] A. S. Thompson,[15] R. Thurman-Keup,[2] P. Tipton,[36] S. Tkaczyk,[11] D. Toback,[39] K. Tollefson,[36] A. Tollestrup,[11] D. Tonelli,[33] H. Toyoda,[29] W. Trischuk,[41] J. F. de Troconiz,[16] J. Tseng,[24] N. Turini,[33] F. Ukegawa,[43] T. Vaiciulis,[36] J. Valls,[38] S. Vejcik III,[11] G. Velev,[11] G. Veramendi,[23] R. Vidal,[11] I. Vila,[7] R. Vilar,[7] I. Volobouev,[23] M. von der Mey,[6] D. Vucinic,[24] R. G. Wagner,[2] R. L. Wagner,[11] N. B. Wallace,[38] Z. Wan,[38] C. Wang,[10] M. J. Wang,[1] B. Ward,[15] S. Waschke,[15] T. Watanabe,[43] D. Waters,[30] T. Watts,[38] R. Webb,[39] H. Wenzel,[20] W. C. Wester III,[11] A. B. Wicklund,[2] E. Wicklund,[11] T. Wilkes,[5] H. H. Williams,[32] P. Wilson,[11] B. L. Winer,[28] D. Winn,[25] S. Wolbers,[11] D. Wolinski,[25] J. Wolinski,[26] S. Wolinski,[25] S. Worm,[27] X. Wu,[14] J. Wyss,[33] W. Yao,[23] G. P. Yeh,[11] P. Yeh,[1] J. Yoh,[11] C. Yosef,[26] T. Yoshida,[29] I. Yu,[21] S. Yu,[32] Z. Yu,[47] A. Zanetti,[42] F. Zetti,[23] and S. Zucchelli[3]

(CDF Collaboration)

[1] *Institute of Physics, Academia Sinica, Taipei, Taiwan 11529, Republic of China*
[2] *Argonne National Laboratory, Argonne, Illinois 60439*
[3] *Istituto Nazionale di Fisica Nucleare, University of Bologna, I-40127 Bologna, Italy*
[4] *Brandeis University, Waltham, Massachusetts 02254*
[5] *University of California at Davis, Davis, California 95616*
[6] *University of California at Los Angeles, Los Angeles, California 90024*
[7] *Instituto de Fisica de Cantabria, CSIC-University of Cantabria, 39005 Santander, Spain*
[8] *Enrico Fermi Institute, University of Chicago, Chicago, Illinois 60637*
[9] *Joint Institute for Nuclear Research, RU-141980 Dubna, Russia*
[10] *Duke University, Durham, North Carolina 27708*
[11] *Fermi National Accelerator Laboratory, Batavia, Illinois 60510*
[12] *University of Florida, Gainesville, Florida 32611*
[13] *Laboratori Nazionali di Frascati, Istituto Nazionale di Fisica Nucleare, I-00044 Frascati, Italy*
[14] *University of Geneva, CH-1211 Geneva 4, Switzerland*
[15] *Glasgow University, Glasgow G12 8QQ, United Kingdom*
[16] *Harvard University, Cambridge, Massachusetts 02138*
[17] *Hiroshima University, Higashi-Hiroshima 724, Japan*
[18] *University of Illinois, Urbana, Illinois 61801*
[19] *The Johns Hopkins University, Baltimore, Maryland 21218*
[20] *Institut für Experimentelle Kernphysik, Universität Karlsruhe, 76128 Karlsruhe, Germany*
[21] *Center for High Energy Physics: Kyungpook National University, Taegu 702-701; Seoul National University, Seoul 151-742; and SungKyunKwan University, Suwon 440-746; Korea*
[22] *High Energy Accelerator Research Organization (KEK), Tsukuba, Ibaraki 305, Japan*
[23] *Ernest Orlando Lawrence Berkeley National Laboratory, Berkeley, California 94720*
[24] *Massachusetts Institute of Technology, Cambridge, Massachusetts 02139*

[25] *University of Michigan, Ann Arbor, Michigan 48109*
[26] *Michigan State University, East Lansing, Michigan 48824*
[27] *University of New Mexico, Albuquerque, New Mexico 87131*
[28] *The Ohio State University, Columbus, Ohio 43210*
[29] *Osaka City University, Osaka 588, Japan*
[30] *University of Oxford, Oxford OX1 3RH, United Kingdom*
[31] *Universita di Padova, Istituto Nazionale di Fisica Nucleare, Sezione di Padova, I-35131 Padova, Italy*
[32] *University of Pennsylvania, Philadelphia, Pennsylvania 19104*
[33] *Istituto Nazionale di Fisica Nucleare, University and Scuola Normale Superiore of Pisa, I-56100 Pisa, Italy*
[34] *University of Pittsburgh, Pittsburgh, Pennsylvania 15260*
[35] *Purdue University, West Lafayette, Indiana 47907*
[36] *University of Rochester, Rochester, New York 14627*
[37] *Rockefeller University, New York, New York 10021*
[38] *Rutgers University, Piscataway, New Jersey 08855*
[39] *Texas A&M University, College Station, Texas 77843*
[40] *Texas Tech University, Lubbock, Texas 79409*
[41] *Institute of Particle Physics, University of Toronto, Toronto M5S 1A7, Canada*
[42] *Istituto Nazionale di Fisica Nucleare, University of Trieste/ Udine, Italy*
[43] *University of Tsukuba, Tsukuba, Ibaraki 305, Japan*
[44] *Tufts University, Medford, Massachusetts 02155*
[45] *Waseda University, Tokyo 169, Japan*
[46] *University of Wisconsin, Madison, Wisconsin 53706*
[47] *Yale University, New Haven, Connecticut 06520*
[(*)] *Now at Carnegie Mellon University, Pittsburgh, Pennsylvania 15213*
[(**)] *Now at Northwestern University, Evanston, Illinois 60208*

Abstract

We present results of searches for diphoton resonances produced both inclusively and also in association with a vector boson (W or Z) using 100 pb^{-1} of $p\bar{p}$ collisions using the CDF detector. We set upper limits on the product of cross section times branching ratio for both $p\bar{p} \to \gamma\gamma + X$ and $p\bar{p} \to \gamma\gamma + W/Z$. Comparing the inclusive production to the expectations from heavy sgoldstinos we derive limits on the supersymmetry-breaking scale $\sqrt{F}$ in the TeV range, depending on the sgoldstino mass and the choice of other parameters. Also, using a NLO prediction for the associated production of a Higgs boson with a W or Z boson, we set an upper limit on the branching ratio for $H \to \gamma\gamma$. Finally, we set a lower limit on the mass of a 'bosophilic' Higgs boson (e.g. one which couples only to γ, W, and Z bosons with standard model couplings) of 82 GeV/c^2 at 95% confidence level.

PACS numbers 13.85Rm, 13.85Qk, 14.80.-j,14.80.Ly

1 Introduction

Many processes in extensions of the standard model (SM) result in final-state signatures involving two vector gauge bosons, $VV + X$, where V is either a W, Z, or photon. The signature of high mass photon pairs is attractive for searches for new physics as the photon is the lightest gauge boson, and hence might be more easily produced in decays of new particles. In addition, the photon, being stable, does not decay into many different final states as do the W and Z. The dominant SM background process, the production of very massive photon pairs ($M_{\gamma\gamma} \gtrsim 100\,\mathrm{GeV/c^2}$), is small compared to the cross-sections for producing new strongly-interacting states via quark-antiquark annihilation, making this an attractive channel in which to search for new particles or interactions. Examples of possible sources of high mass diphoton pairs include sgoldstino production [1], interaction terms arising from extra spatial dimensions [2], a new interaction at a high scale manifesting itself as a $q\bar{q} \to \gamma\gamma$ contact interaction [3], a 'bosophilic' Higgs boson [4, 5, 6, 7], or a heavy analog of the π^0 that also does not couple to fermions [8]. In this paper we focus on the production of sgoldstinos and Higgs bosons and their decay into two photons.

Models with spontaneous breaking of global supersymmetry require a massless and neutral spin-$\frac{1}{2}$ particle, goldstino ($\tilde{G}$). When gravitation is added and supersymmetry is realized locally the gauge particle, the graviton, has a spin-$\frac{3}{2}$ partner, the gravitino, which acquires a mass while the goldstino is absorbed [9]. Goldstinos (R-odd) have supersymmetric partners called sgoldstinos (R-even) which are expected to be a part of the effective theory at the weak scale if gravitinos are very light ($\lesssim 10^{-3}$ eV/c^2). The simplest model considers two neutral spin-0 states: S (CP-even) and P (CP-odd), for which we use the generic symbol ϕ. The mass for these states is completely arbitrary and although initially signals were studied in the limit of vanishing masses [10], we follow the suggestions of Ref. [1] and concentrate on massive sgoldstinos, $M_\phi = \mathcal{O}(100\ \mathrm{GeV/c^2})$. The production of sgoldstinos is dominated by the gluon-gluon fusion process [1] while their decay is dominated by two-body decays into a pair of gluons, goldstinos, photons, W's, Z's and top quarks. The corresponding branching ratios have been calculated [11] for two specific choices of parameters, the branching ratio into two photons being of the order of a few percent. Limits on the supersymmetry-breaking scale $\sqrt{F}$ have been set by the DELPHI Collaboration [12] for sgoldstino masses up to about 200 GeV/c^2. We take advantage here of the higher energy reached at the Tevatron to extend the search to much larger masses.

There are also models in which a Higgs boson could decay into two photons with a branching ratio much larger than predicted in the standard model. Figure 1 shows the dominant diagrams for production of a standard model Higgs boson (H) in $p\bar{p}$ collisions. The total production cross section is dominated by the gluon-gluon fusion process, and has a value of approximately 1 pb for $M_H \sim 100$ GeV/c^2 [5, 13]. Figure 2 shows the dominant decay diagrams for a SM Higgs with mass less than $\sim$130 GeV/c^2. The dominant decay mode of the H in this mass range is $H \to b\bar{b}$, with the branching ratio to $\gamma\gamma$ being on the order of 10^{-4}. At higher masses, the decays to vector boson pairs WW and

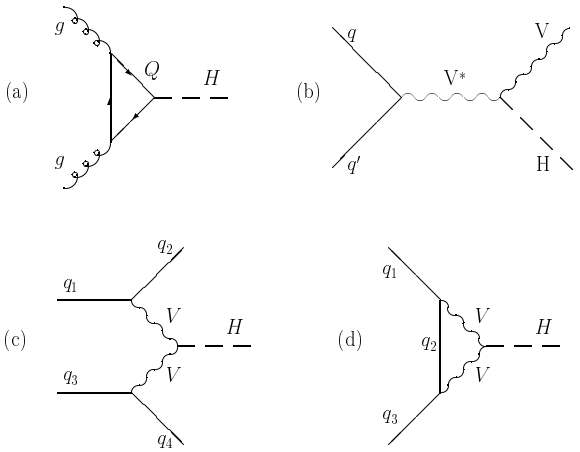

Figure 1: Diagrams for production of a Higgs Boson in $p\bar{p}$ collisions: (a) gluon-gluon fusion, (b) associated production with a vector boson, (c) and (d) vector boson fusion. In the bosophilic models the gluon-gluon fusion diagram is suppressed.

ZZ dominate. However, some models beyond the standard model introduce anomalous couplings [14] or additional Higgs multiplets [5, 7], enhancing the coupling to photons or suppressing the coupling to fermions. The result is a low-mass Higgs boson with significantly increased branching ratio to two photons. In the bosophilic models, the coupling to fermions at tree level is set to zero while maintaining the SM coupling to vector bosons. Although the decay to two photons proceeds through a higher-order loop diagram, it is the dominant decay for $M_H < M_W$. For $M_H > M_W$ the decay $H \to WW^*$ becomes dominant. Since the bosophilic Higgs has no coupling to fermions, the gluon-gluon fusion production mechanism is lost and the dominant production mode in $p\bar{p}$ collisions at $\sqrt{s} = 1.8$ TeV is associated production with a W or Z boson. For $M_H = 80$ GeV/c^2, the total associated production cross section is about 0.8 pb. The limit set in this paper uses the branching ratios of reference [5].

Limits on the mass and branching ratios of a bosophilic Higgs boson have been set by the OPAL Collaboration assuming SM production of ZH with a lower limit on M_H of 96.2 GeV/c^2 at 95% confidence level (C.L.) [15]. More recently, a limit of 100.7 GeV/c^2 at 95% C.L. [16] has been set by the ALEPH Collaboration. The D0 Collaboration at Fermilab has set a lower limit of 78.5 GeV/c^2 at 95% C.L. [17] in a search at the Tevatron for WH and ZH production.

In this paper we describe a search for departures from SM expectations for both inclusive high-mass $\gamma\gamma$ production and also $\gamma\gamma$ production in association with a W or Z boson. This search uses 100 ± 4 pb^{-1} of data collected between 1992 and 1995 with the Collider Detector at Fermilab (CDF). The photon se-

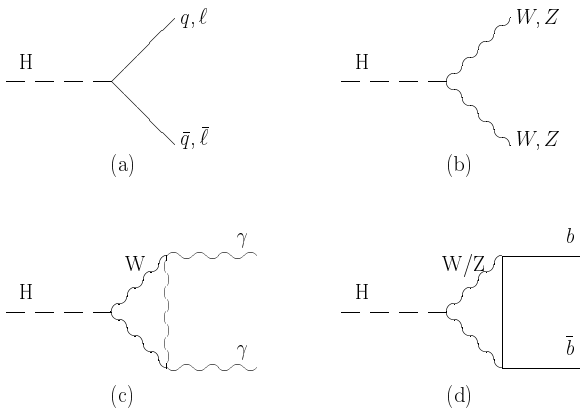

Figure 2: Diagrams for the decay of a Higgs Boson to: (a) a quark or lepton pair, (b) vector boson pairs (WW/ZZ), (c) via a loop to $\gamma\gamma$, and (d) via a loop to $b\bar{b}$. For a bosophilic Higgs, the decay to $b\bar{b}$ is suppressed relative to $\gamma\gamma$.

lection criteria for this analysis were optimized to remain efficient for very high energy photons. The analysis is complementary to the previous QCD diphoton cross section measurement [18]. In this present analysis, the photon selection criteria have been optimized for high efficiency, taking advantage of the smaller jet fake background rate at high E_T. The analysis is also complementary to the recent diphoton + X search analysis [19] which searched for non-resonant diphoton signatures, such as $ee\gamma\gamma\not\!\!E_T$, that might arise in gauge-mediated supersymmetric models.

2 The CDF Detector

We briefly describe the CDF detector, which is described in detail elsewhere [20]. The magnetic spectrometer consists of three tracking devices immersed in the 1.4 T field of a 3 m-diameter 5 m-long super-conducting solenoid. The magnetic field and three tracking devices are all arranged with their principal axis parallel to the proton beam direction (z-axis) [21]. The tracking device closest to the beam line is a four-layer silicon micro-strip vertex detector (SVX), used to find secondary vertices, with layers at radii from 2.8 cm to 7.9 cm [22]. Surrounding the SVX is a set of time projection chambers (VTX) which identifies the $p\bar{p}$ interaction point(s) along the beam axis with a series of $r-z$ measurements out to a radius of 22 cm. The central tracking chamber (CTC) is a 3.5 m-long 84 layer drift chamber surrounding the VTX. The CTC wires, ranging in radius from 31.0 cm to 132.5 cm, are arranged in 5 superlayers of axial wires alternating with 4 superlayers of stereo wires. The calorimeter, which is constructed in projective electromagnetic and hadronic towers, consists of the central barrel ($|\eta| < 1.1$) which surrounds the solenoid, the end-plugs ($1.1 <$

$|\eta| < 2.4$) which form the magnet poles and the forward calorimeters($2.4 < |\eta| < 4.2$). Wire chambers with cathode strip readout (CES) are located at shower maximum in the central electromagnetic calorimeter. These chambers provide a two-dimensional shower profile which is used to discriminate on a statistical basis between photons and π^0 backgrounds. Additional statistical discrimination is provided by exploiting the difference in conversion probability for single photons and pairs from π^0 decays in the 1 radiation length of the coil. The presence of a conversion is detected using wire chambers (CPR) located between the coil and the central calorimeter. The central muon chambers ($|\eta| < 1.1$) are located outside the central calorimeter to detect particles penetrating the calorimeter.

3 Diphoton Event Selection

Photons are identified as a narrow shower in the electromagnetic calorimeter with no associated high-P_T charged particle track. The energy in the hadronic calorimeter and adjoining regions of the electromagnetic calorimeter must be small to reject jet backgrounds. For high-E_T photons there is a background from $\pi^0 \to \gamma\gamma$ decays where both photons are very close together.

The candidate $\gamma\gamma$ events must pass the diphoton requirements of the three-level CDF trigger. The first hardware level requires two central electromagnetic calorimeter trigger towers with $E_T > 4$ GeV. The second hardware level requires two central electromagnetic trigger clusters [23] with $E_T > 16$ GeV and a ratio of hadronic to electromagnetic energy satisfying $E_T(HAD)/E_T(EM) < 0.125$. In the third trigger level, electromagnetic clusters [24] are found using the offline reconstruction algorithm and the 16 GeV threshold is re-applied to the recalculated transverse energy of the new cluster.

Offline event selection requires at least two central electromagnetic clusters each satisfying the following requirements: $E_T > 22$ GeV, no track pointing at the cluster (or one track with $P_T < 1$ GeV/c), pulse height and cluster shape in the central electromagnetic strip chamber (CES) consistent with a photon (to reject π^0's and cosmic rays), no additional CES cluster in the same 15° azimuthal section of the calorimeter (to reject π^0's), and minimal energy deposited in the hadronic calorimeter towers behind the cluster.

Isolation requirements, based on track and calorimeter activity in an $\eta - \phi$ cone with radius $\Delta R \equiv \sqrt{(\Delta\phi)^2 + (\Delta\eta)^2} = 0.4$ around the cluster, are used to reduce backgrounds from jets: $\Sigma P_T(Tracks) < 5.0$ GeV/c and $(E_T(\Delta R < 0.4) - E_T(Cluster)) < 2.0$ GeV. The calorimeter isolation energy is corrected for leakage from the cluster and for pile-up from multiple interactions. The efficiency of the calorimeter isolation requirement is studied as a function of E_T using a sample of electrons from $W \to e\nu$ events. The efficiency for electrons with $30 < E_T < 100$ GeV is $94.0 \pm 0.1\%$ and for electrons with $100 < E_T < 200$ GeV is $94.9 \pm 0.6\%$. Two requirements reject backgrounds from cosmic rays: there must be at least one reconstructed primary vertex within ± 60 cm of the center of the interaction region along the beam direction, and all energy measured in the central hadronic calorimeters is required to be in time with the collision.

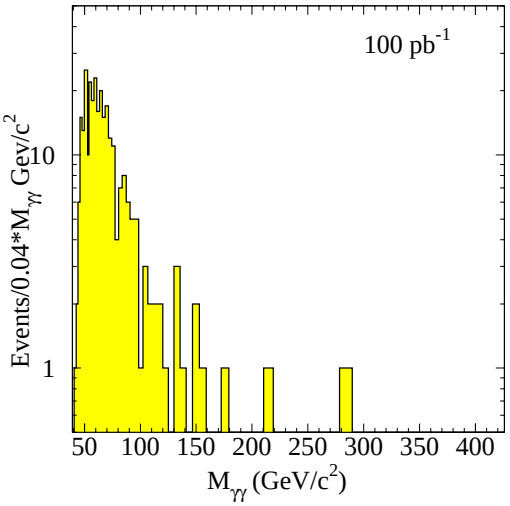

Figure 3: The invariant mass distribution of diphoton candidates (287 events) with a bin-width of 4% of the mass. Note that the three highest-mass bins contain one event each.

The efficiency to identify a photon passing the above isolation criteria within the fiducial region of the central calorimeter is measured using a control sample of electrons from Z^0 decay to be $84 \pm 4\%$. The combined diphoton and event selection efficiency is $63 \pm 6\%$ (the geometric factor due to the fiducial region is subsumed into the geometric and kinematic acceptances, calculated from the Monte Carlo simulation of the detector, as described below).

Figure 3 shows the invariant mass distribution of the 287 diphoton candidate events that pass the selection criteria. A variable bin-width has been chosen to correspond to two times the mass resolution (2σ) to enable the observation of narrow structures.

4 Backgrounds

The dominant backgrounds for this analysis are $\gamma-$jet and jet-jet production, where the jets have 'faked' photons by fluctuating to a single π^0 or η, and real photon pairs from prompt QCD production. The estimated background from $Z^0 \to e^+e^-$ with both electrons faking photons is less than 1 event.

The jet fake rate is measured directly from the data using methods developed for measurements of the inclusive photon [25] and di-photon cross-sections [18]. For clusters with $E_T < 35$ GeV, the lateral shape of the shower in the CES system is used to discriminate between prompt photons and photons from

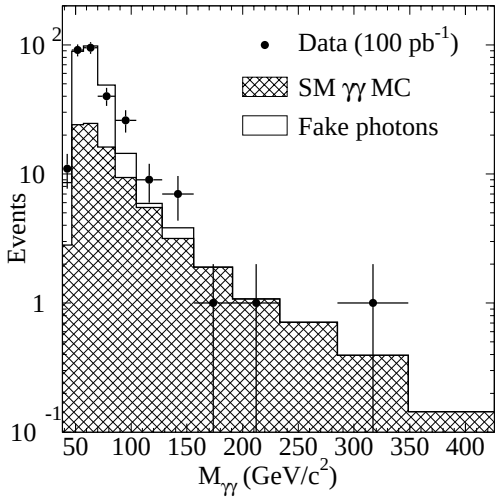

Figure 4: The diphoton candidate mass distribution is compared with background predictions with a bin-width of 20% of the mass. The shaded distribution represents the Monte Carlo prediction for QCD diphoton production; the unshaded distribution represents the predicted yield for jets faking photons.

$\pi^0 \to \gamma\gamma$. Above 35 GeV, where the shapes of showers in the CES from photons and π^0s are indistinguishable, the difference in conversion probability of a single photon and a pair of photons (from π^0 decay) in the material of the magnet coil in front of the CPR chambers is used to calculate the single-photon purity. These probabilities are used to calculate weights for each event being 'photon-photon', 'photon-fake' or 'fake-fake'. The result of applying this method to the sample of 287 event diphoton candidates is that $183 \pm 56 \pm 32$ events are 'photon-fake' or 'fake-fake'. This corresponds to a background fraction of $64 \pm 19 \pm 11\%$, where the first uncertainty is statistical and the second is systematic. The systematic uncertainty comes primarily from uncertainties in the modeling of the backscattering of photons from the electro-magnetic shower in the calorimeter into the CPR chambers, and the modeling of the shower shapes in the CES chambers.

The mass spectrum of the jet fakes is determined using a control sample of events enriched in fake photons. This sample is made using the same selection requirements as the diphotons except that one or both clusters fail the calorimeter isolation requirement. This sample contains some real diphotons which fail the isolation requirement. From studies of high-E_T electrons from W and Z decays, we estimate that 10% of diphoton signal events will end up in the non-isolated sample. The mass distribution of the 198 event non-isolated sample is normalized to the number of fake events measured in the diphoton

candidate sample (183 events).

Two standard model processes make significant contributions to prompt diphoton production: $q\bar{q} \to \gamma\gamma$ and $gg \to \gamma\gamma$. In addition, initial and final state electromagnetic radiation from $\gamma-$jet production contributes indirectly to the diphoton mass spectrum. In the indirect case, several processes contribute to $\gamma-$jet production: $q\bar{q} \to g\gamma$, $qg \to q\gamma$, and $qq \to g\gamma$. These standard model processes are modeled using the Monte Carlo program PYTHIA [26] with CTEQ4L structure functions [27] and the CDF fast detector simulation. The $\gamma\gamma$ event selection efficiency is determined using the MC and detector simulation, with a correction factor of $C_{MC} \equiv 0.76 \pm 0.08$ applied to account for differences between the detector simulation and the actual detector performance. These differences are dominated by effects from additional low energy tracks from the underlying event and from track reconstruction. The correction factor is obtained by comparing the efficiency of the photon selection requirements when applied to electrons from $Z^0 \to e^+e^-$ events from Monte Carlo and data. The $Z^0 \to e^+e^-$ events are selected with very loose requirements to minimize any bias in the method. A global systematic uncertainty of $13-16\%$ applies to these estimates, coming from the uncertainty on the correction factor (10%), the modeling of QED radiation (10% for diphoton masses below 120 GeV/c^2 and 5% above), the dependence on the structure functions (5%), and the integrated luminosity (4%).

The total predicted background from fake photons plus QCD diphoton production is 280 ± 66 events. Figure 4 shows a comparison of the diphoton mass spectrum for the 287 isolated diphoton candidates (points) with background predictions. The shaded distribution represents the standard model diphoton prediction from the PYTHIA Monte Carlo program, while the unshaded distribution represents the predicted spectrum from jets faking photons. The bin-width in this plot corresponds to about 10 times the mass resolution; any narrow-width resonance would be seen in the finer binning of Figure 3. The data are well-modeled by the background predictions: above 70 (100) GeV/c^2 we observe 85 (21) events compared to a background prediction of 77.1 ± 15.7 (14.7 ± 3.2) events. The numbers of events and backgrounds are summarized in Table 1.

5 Limit on Inclusive $\gamma\gamma$ Production

We first consider the signature of $\gamma\gamma$ +X. We set limits on the cross section for narrow resonances with mass greater than 70 GeV/c^2 [28]. The acceptance for diphoton production is evaluated using the diphoton decay of a narrow resonance, $\phi \to \gamma\gamma$, as a model of the kinematics for the production and decay of a heavy sgoldstino. The sgoldstino samples are generated using the PYTHIA Monte Carlo generator with CTEQ4M structure functions [27], simulated using the CDF fast detector simulation, and passed through the same event selection criteria as the data. The product of efficiency times acceptance increases from 10% at 75 GeV/c^2 to 16% at 400 GeV/c^2. The correction factor C_{MC} dis-

Mass (GeV/c^2)	Events Photons	Fake Production	SM	Total	ϵA	σ (pb)
46.8-57.2	90	65.2 ± 23.8	24.1 ± 3.9	89.3 ± 24.1	0.04	–
57.2-70.0	95	73.3 ± 26.7	24.6 ± 3.9	97.9 ± 27.0	0.07	–
70.0-85.6	40	32.6 ± 12.5	16.2 ± 2.6	48.8 ± 12.7	0.107	2.25
85.6-104.6	26	5.0 ± 2.6	9.4 ± 1.5	14.4 ± 3.0	0.112	2.12
104.6-127.8	9	$0.4^{+1.0}_{-0.4}$	5.5 ± 0.9	$5.9^{+1.3}_{-1.0}$	0.119	0.90
127.8-156.2	7	$0.6^{+1.0}_{-0.6}$	3.2 ± 0.4	$3.8^{+1.1}_{-0.7}$	0.126	0.80
156.2-191.0	1	< 0.04	1.9 ± 0.3	1.9 ± 0.3	0.134	0.30
191.0-233.4	1	–	1.1 ± 0.2	1.1 ± 0.2	0.143	0.29
233.4-285.2	0	–	0.7 ± 0.1	0.7 ± 0.1	0.151	0.20
285.2-348.6	1	–	0.4 ± 0.1	0.4 ± 0.1	0.158	0.29
348.6-426.0	0	–	0.1 ± 0.1	0.1 ± 0.1	0.163	0.19
Total	270	177.1 ± 62.3	87.2 ± 14.4	264.3 ± 63.9	–	–

Table 1: The number of diphoton events observed, background from jets faking photons, 'background' from standard model diphoton production, total background, efficiency times acceptance, and 95% C.L. cross section limit for $\gamma\gamma + X$ production for each mass bin. Mass bins have a width of 20% of the bin center. The first two bins are not used for cross section limits, due to their low acceptance.

cussed above is applied to the $\gamma\gamma$ efficiency. The acceptance has an additional systematic uncertainty of 4% due to the dependence on the structure functions.

The cross section limit in each mass bin of Table 1 above 70 GeV/c^2 is given by the following expression:

$$\sigma(p\bar{p} \to \gamma\gamma) < \frac{N^{95\%\ CL}(\gamma\gamma)}{\epsilon \cdot\ A \cdot \int \mathcal{L}dt} \tag{1}$$

where $N^{95\%\ CL}(\gamma\gamma)$ is the 95% C.L. upper limit on the number of diphoton events in the mass bin, ϵ is the selection efficiency, A is the acceptance evaluated in the center of the bin, and $\int \mathcal{L}dt$ is the integrated luminosity. The upper limit on the number of events in each bin is determined using a Monte Carlo technique [29] which convolutes the uncertainties (including systematic uncertainties) on acceptance, efficiency and the integrated luminosity with the background expectations. The total systematic uncertainty of 12% consists of 4% from the luminosity measurement, 10% from the selection efficiencies, and 4% from the acceptance. Table 1 provides a summary of the limits. Figure 5 shows the cross section limits in nine mass bins above 70 GeV/c^2. For comparison, the cross section times branching ratio for $p\bar{p} \to H^0 + W/Z \to \gamma\gamma + X$ production is shown (dashed curve) for bosophilic branching ratios [5]. The curve corresponding to the standard model branching ratio is not shown, being at least one order of magnitude below the bosophilic one.

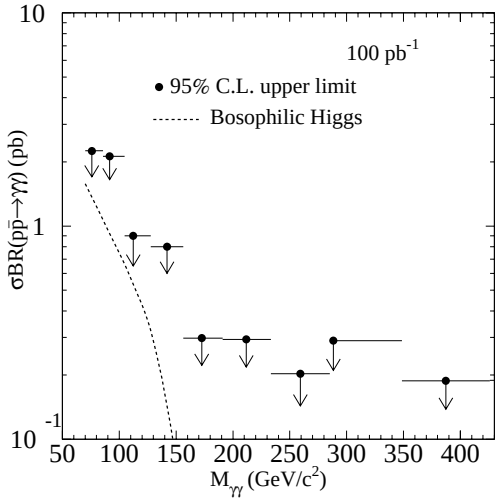

Figure 5: Cross section limit at 95% C.L. for high mass diphoton production from a resonant state with negligible natural width. The points represent the average mass of the events in each bin, but the limits are evaluated at the bin center. The theoretical cross section for a bosophilic Higgs boson [5] is shown as a dashed line.

5.1 Limits on the production of heavy sgoldstinos

In the scenario in which squarks, sleptons, gluinos, charginos, neutralinos and Higgs bosons are sufficiently heavy not to play any rôle in sgoldstino decays, the most important decays are the two-body decays: $\phi \to \tilde{G}\tilde{G}, \gamma\gamma, gg, \gamma Z, ZZ, W^+W^-$ and $f\bar{f}$. Three and four-body decays are also possible but quite suppressed. Sgoldstino couplings can be parameterized in terms of the supersymmetry breaking scale $\sqrt{F}$, the gaugino masses, M_3, M_2 and M_1, and a mass parameter, μ_a, associated with the charged higgsino. To account for the $t\bar{t}\phi$ coupling for heavy sgoldstinos, two arbitrary free parameters, A_S and A_P, with the dimension of a mass are introduced. We adopt in the following the two sets of choices for the parameters adopted in Ref. [11]: these choices represent a situation in which sgoldstino production is more important than gluino/chargino/neutralino production. The two sets correspond to chargino masses of about (220, 380) for case A and about (270, 430) GeV/c^2 for case B. In order for the calculations to be valid, the sgoldstino total width has to be small compared to m_ϕ. For both parameter sets the decay $\phi \to gg$ dominates, but $\phi \to \gamma\gamma$ is not negligible, being of the order of few percent.

The dominant mechanism for sgoldstino production is gluon-gluon fusion $g + g \to \phi$, while other associated processes such as $q + \bar{q} \to V + \phi$ ($V =$

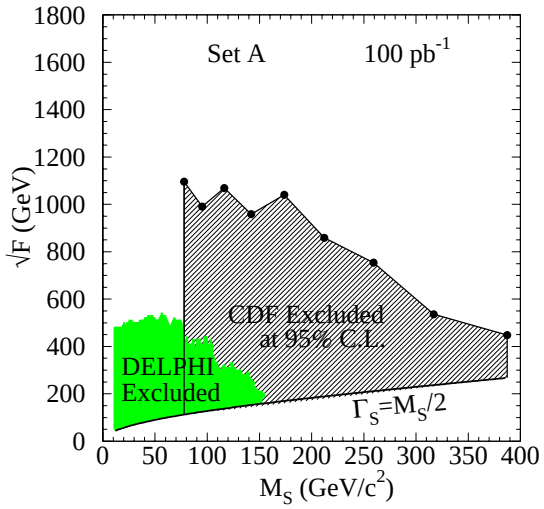

Figure 6: The exclusion region at the 95% C.L. for S-type (CP-even) sgoldstinos in the M_S-$\sqrt{F}$ space for the parameters of set A: $M_3 = A_S = A_P = 400$, $M_2 = \mu_a = 300$,$M_1 = 200$ GeV/c^2. M_S is mass of the S-type sgoldstino. The CDF results are shown as the hatched area; the region excluded by results from DELPHI [12] is shown as the solid shaded area. The points represent the mass at which the limits are calculated. The boundary $\Gamma_S = M_S/2$ beyond which the model may not be valid is also shown.

γ, W, Z) or $q + \bar{q} \to q + \bar{q} + \phi$ are suppressed by about four orders of magnitude. The calculation of the production cross section has been made at lowest order (LO) [1]; however NLO QCD corrections to $\sigma(p\bar{p} \to \phi) \times BR(\phi \to \gamma\gamma)$ are expected to be negligible because they have cancelling effects in the cross section and branching ratio.

Comparing the limits found on the inclusive production cross section to the theoretical value of $\sigma(p\bar{p} \to \phi) \times BR(\phi \to \gamma\gamma)$ bin-by-bin, and considering its $1/F^2$ dependence, we derive lower limits on $\sqrt{F}$ for sgoldstino masses corresponding to the center of the bin. These limits are represented as exclusion regions in the M_ϕ vs $\sqrt{F}$ space. Figures 6 and 7 show these limits for the S-type sgoldstinos. The limits for the P-type (CP-odd) sgoldstino are very similar, differing by less than 0.1%. No limit is set in the region $\Gamma_\phi > M_S/2$, where the theoretical calculation may not be valid [1].

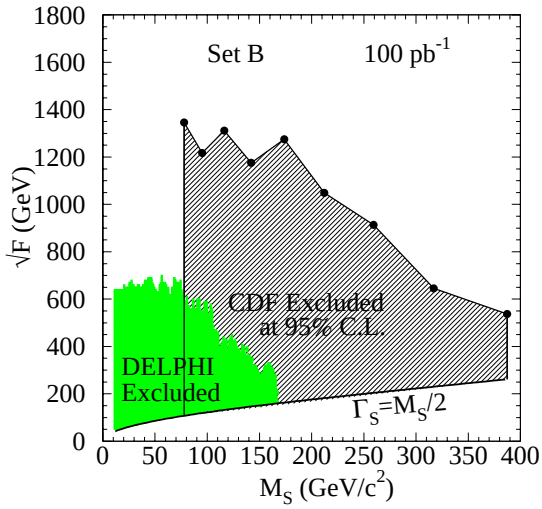

Figure 7: Exclusion region at the 95% C.L. in the M_S-$\sqrt{F}$ space for the parameters of set B: $M_3 = M_2 = M_1 = \mu_a = A_S = A_P = 350$ GeV/c^2. The CDF results are shown as the hatched area; the region excluded by results from DELPHI [12] is shown as the solid shaded area. The points represent the mass at which the limits are calculated. The boundary $\Gamma_S = M_S/2$ beyond which the model may not be valid is also shown.

6 Selecting $\gamma\gamma$ + W/Z Candidates

The inclusive $\gamma\gamma$ analysis is not sensitive to production of a bosophilic Higgs decaying to two photons in the lower-mass region 60-100 GeV/c^2 because the backgrounds from jets faking photons and QCD diphoton production are too high (see Figure 5). To increase sensitivity in this mass region we narrow the signature to be $\gamma\gamma + W/Z$. The additional requirement of a W or Z boson significantly reduces these backgrounds, allowing access to smaller cross sections.

To achieve a high acceptance for all W and Z decay channels, the vector bosons are selected using simple signatures which yield significant background reductions without the inefficiency of full reconstruction. The backgrounds from jet fakes and QCD $\gamma\gamma$ production are evaluated using the non-isolated sample of 198 events and PYTHIA Monte Carlo QCD background sample used in the inclusive $\gamma\gamma$ analysis previously described. Backgrounds from electroweak processes are found to be insignificant.

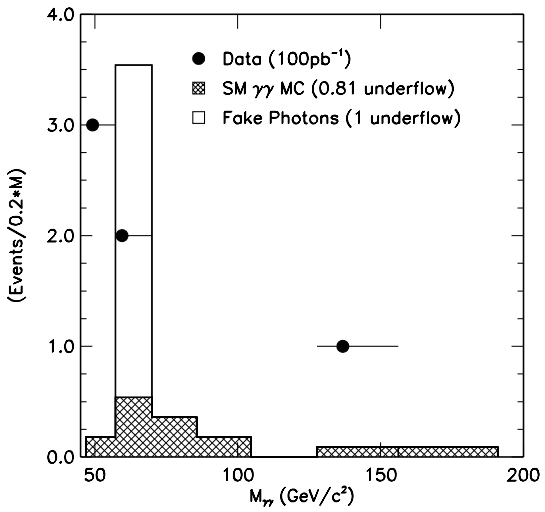

Figure 8: Photon-photon mass distribution compared with background predictions for events passing the $\gamma\gamma + W/Z$ selection. The cross-hatched distribution represents the Monte Carlo prediction for QCD diphoton production; the shaded one represents the predicted yield from jets faking photons. The choppy appearance of the background estimates is the result of low efficiency for the W/Z selection. The small electroweak backgrounds are not shown.

The vector boson selection consists of the logical OR of three general categories based on decay channels as follows:

1. Central isolated electron ($E_T > 20$ GeV) or muon ($P_T > 20$ GeV/c) for $W \to l\nu$ and $Z^0 \to l^+l^-$
2. $\not\!\!E_T > 20$ GeV for $W \to l\nu$ and $Z^0 \to \nu\bar{\nu}$
3. Two Jets ($E_T > 15$ GeV, $|\eta| < 2.0$) for $W \to qq'$ and $Z^0 \to q\bar{q}$

where $\not\!\!E_T$ is the symbol for missing transverse energy [30].

Leptons (e and μ) are selected using the isolated central lepton requirements used in the 'lepton-plus-jets' analysis for the discovery of the top quark [31]. The lepton identification efficiencies are measured in data samples of Z bosons decaying to electrons ($77.8 \pm 0.6\%$) and muons ($90.6 \pm 0.5\%$). The missing transverse energy is corrected for any high-P_T central muons. Since mismeasured jet energies can result in false $\not\!\!E_T$, events with any jet ($E_T^{\rm jet} > 10$ GeV) within 25° of the $\not\!\!E_T$ direction are rejected. Jets are identified in the calorimeter using a fixed cone algorithm [32] with a cone size in η-ϕ space of radius $\Delta R = 0.4$. Any jet

Set	M_3	M_2	M_1	μ_a	A_S	A_P	units
A	400	300	200	300	400	400	GeV/c^2
B	350	350	350	350	350	350	GeV/c^2

Table 2: The two sets of mass parameters used in the sgoldstino theoretical cross section calculations.

Selection	Isolated Sample	Background Estimate
Two Isolated Photons $E_T^\gamma > 22$ GeV	287	280 ± 66
Central Electron, $E_T > 20$ GeV	1	0.2 ± 0.2
Central Muon, $P_T > 20$ GeV/c	0	0
$\not\!\!E_T > 20$ GeV	3	1.8 ± 1.3
2 Jets ($E_T > 15$ GeV, $40 < M_{JJ} < 130$ GeV/c^2)	3	4.6 ± 1.9
Any W/Z signature	6	6.4 ± 2.1

Table 3: Summary of the $\gamma\gamma$ + W/Z candidate events. The number of $\gamma\gamma$ candidate events passing each of the W/Z selection requirements are listed. There is one event which passes both the jet-jet and $\not\!\!E_T$ selection requirements. The background estimates come primarily from fakes (non-isolated control sample) plus SM $\gamma\gamma$ production with a small contribution from electroweak sources. Some background events pass more than one of the W/Z selections.

within a radius of 0.4 in η-ϕ space of an electron or within a radius of 0.6 of a photon is ignored. Finally the jet-jet invariant mass is required to be consistent with a W or Z boson: $40 < M_{JJ} < 130$ GeV/c^2.

The results of the $\gamma\gamma + W/Z$ event selection are summarized in Table 3 listing the number of events satisfying each W/Z selection requirement. Some properties of the 6 events passing the selection requirements are listed in Table 4 including one event which passes both the jet-jet and $\not\!\!E_T$ selection requirements. The highest mass event has a $\gamma\gamma$ invariant mass of 137 GeV/c^2 and $\not\!\!E_T$ = 21 GeV. The total estimated background for $M_{\gamma\gamma} > 130$ GeV/c^2 is 0.19 ± 0.12 events.

Table 3 also lists the estimated backgrounds from photon fakes, QCD $\gamma\gamma$ production, and electroweak sources, which total 6.4 ± 2.1 events. Fake-photon backgrounds, which are estimated from the non-isolated data sample, contribute 1 event to the $\not\!\!E_T$ category and 3 events to the jet-jet category. Backgrounds from QCD $\gamma\gamma$, which are estimated using a sample generated with the Pythia Monte Carlo equivalent to 1 fb^{-1} of data, contribute 0.8 events to the $\not\!\!E_T$ category and 1.6 events to the jet-jet category[1]. There are small electroweak backgrounds, 0.2 ± 0.2 events which contribute to the electron signature from events with a W or Z boson produced in association with multiple photons

[1]There is a small overlap between signatures for the QCD $\gamma\gamma$ background.

and/or jets. These events only contribute in the case where the $W(Z)$ decays to an electron(s) and the charged track(s) associated with the electron(s) is not reconstructed. Figure 8 shows the $\gamma\gamma$ mass distribution of events passing all $\gamma\gamma + W/Z$ selection for the isolated diphoton data and the background samples. The mass distribution for the electroweak events is neglected. There is no evidence of a $\gamma\gamma$ resonance in the data.

Run	Event	Channel(s)	$M_{\gamma\gamma}$ (GeV/c^2)	Properties
45219	277283	$\not\!\!E_T$,jet-jet	59.1	$\not\!\!E_T = 28.8$ GeV, $M_{JJ} = 96.1$ GeV/c^2
60597	119813	$\not\!\!E_T$	136.8	$\not\!\!E_T = 20.8$ GeV
61514	9698	Jet-jet	48.9	$M_{JJ} = 75.1$ GeV/c^2
68739	257646	Electron	47.1	$\not\!\!E_T = 36.1$ GeV, $\not\!\!E_T = 52.8$ GeV
68847	264160	Jet-jet	59.9	$M_{JJ} = 74.6$ GeV/c^2
70019	155639	$\not\!\!E_T$	51.7	$\not\!\!E_T = 22.0$ GeV

Table 4: Features of the six events passing the $\gamma\gamma + W/Z$ selection requirements.

7 Limits on $\gamma\gamma$ + W/Z Production

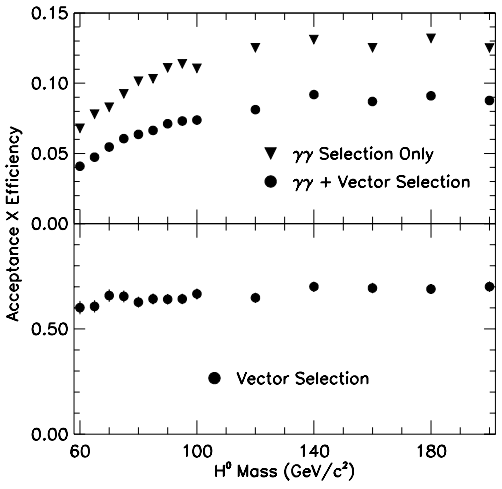

Figure 9: Acceptance×efficiency for VH production, with the W and Z bosons decaying via any SM decay and the Higgs boson decaying to $\gamma\gamma$.

We set an upper limit on the cross section times branching ratio for the process $p\bar{p} \to \gamma\gamma + W/Z$ as a function of $\gamma\gamma$ mass:

$$\sigma(p\bar{p} \to \gamma\gamma + W/Z) < \frac{N^{95\% CL}(\gamma\gamma + W/Z)}{\epsilon \cdot \ A \cdot \int \mathcal{L}dt} \tag{2}$$

where $N^{95\% \ CL}(\gamma\gamma + W/Z)$ is the 95% C.L. upper limit on the number of events, $\epsilon \cdot A$ is the product of efficiency times acceptance, and $\int \mathcal{L}dt$ is the integrated luminosity. The number of signal events at each mass is taken as the number of isolated diphoton events passing the vector (W/Z) selection cuts and falling within a $\pm 3\sigma(M_H)$ mass window around the candidate mass, σ being about 2 (3) GeV/c^2 for $M_H = 100$ (150) GeV/c^2. We calculate $N^{95\% \ CL}$ at each mass, assuming no background subtraction and including a Gaussian systematic uncertainty of 15% which includes diphoton selection efficiency (10%), luminosity (4%), gluon radiation modeling (11%), and jet energy scale (7%).

The acceptance is determined from Monte Carlo samples of associated Higgs + W/Z generated with PYTHIA and CTEQ4L structure functions [27]. Figure 9 shows the product of the efficiency times acceptance as a function of M_H before and after the vector boson selection cuts. The efficiency times acceptance increases from about 4% for $M_H = 60$ GeV/c^2 to about 9% for $M_H > 100$ GeV/c^2. The mass dependence of the acceptance is dominated by the photon E_T requirement.

Figure 10 shows the 95% C.L. upper limit on the cross section times branching ratio for $p\bar{p} \to \gamma\gamma + W/Z$. The overlayed dashed curve is the prediction for a bosophilic Higgs using the branching ratios from reference [5] and a NLO cross section calculation from reference [13], using the CTEQ4M structure functions [27]. A 95% C.L. lower limit on the mass of a bosophilic Higgs is set at 82 GeV/c^2. Table 5 provides a summary of the limit.

An upper limit on the branching fraction for $H \to \gamma\gamma$ is obtained by dividing the cross section limit on $\gamma\gamma + W/Z$ by the predicted cross section for $W/Z + H$ production. The resulting branching ratio upper limit is shown in Figure 11. The overlayed dashed and dotted curves are the predictions for a bosophilic and Standard Model Higgs boson (scaled up by a factor of 100), respectively.

8 Conclusions

We have presented results of searches for massive diphoton production both inclusively and in association with a high-P_T lepton, $\not\!\!E_T$, or dijets. The latter channels are sensitive to production of a vector boson in association with a Higgs boson which subsequently decays to photons. Both the inclusive and exclusive signatures are consistent with predictions from standard model sources. In the inclusive channel we set upper limits on the production of narrow resonances decaying into two photons. Comparing these limits to a LO calculation for massive sgoldstino production we set limits in the range of 1 TeV on the supersymmetry-breaking scale $\sqrt{F}$ for two sets of parameters. In the exclusive

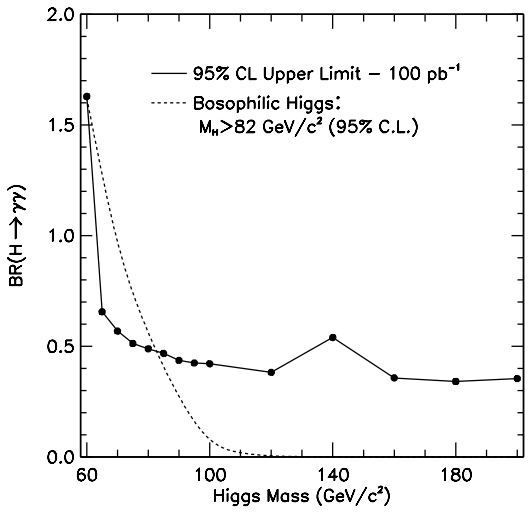

Figure 10: Upper limit at 95% C.L. on the $\gamma\gamma + W/Z$ cross section as a function of $\gamma\gamma$ mass. The dashed curve shows the prediction for cross section times branching fraction for a bosophilic $H \to \gamma\gamma$ with branching fraction from reference [5] and the cross section for associated Higgs production is a Standard Model NLO calculation from reference [13].

channels, we set an upper limit on the cross section times branching fraction for $p\bar{p} \to \gamma\gamma + W/Z$ between 60 and 200 GeV/c^2. Using a NLO calculation of the SM cross section for $p\bar{p} \to VH$ we set a 95% C.L. upper limit on the branching ratio for $H \to \gamma\gamma$. Between approximately 60 and 100 GeV/c^2 the upper limit on the branching ratio is less than 1. Using the branching ratios of reference [5] the lower limit on the mass of a bosophilic Higgs is 82 GeV/c^2 at 95% C.L.

9 Acknowledgments

We thank the Fermilab staff and the technical staffs of the participating institutions for their vital contributions. This work was supported by the U.S. Department of Energy and National Science Foundation; the Italian Istituto Nazionale di Fisica Nucleare; the Ministry of Education, Science and Culture of Japan; the Natural Sciences and Engineering Research Council of Canada; the National Science Council of the Republic of China; the Swiss National Science Foundation; and the A.P. Sloan Foundation.

$M_{\gamma\gamma}$ (GeV/c^2)	$\epsilon \times A$	$d\sigma/dM_{\gamma\gamma}$ (pb/GeV^2)
60	0.048±0.002	1.65
65	0.047±0.002	0.66
70	0.055±0.002	0.57
75	0.061±0.002	0.52
80	0.064±0.002	0.49
85	0.066±0.002	0.47
90	0.071±0.002	0.44
95	0.073±0.002	0.43
100	0.074±0.002	0.42
120	0.081±0.002	0.39
140	0.092±0.002	0.54
160	0.087±0.002	0.36
180	0.091±0.002	0.36
200	0.088±0.002	0.36

Table 5: Diphoton mass, efficiency (ϵ) times acceptance (A), and cross section limit (95% C.L.) for associated W/Z + high mass diphoton production.

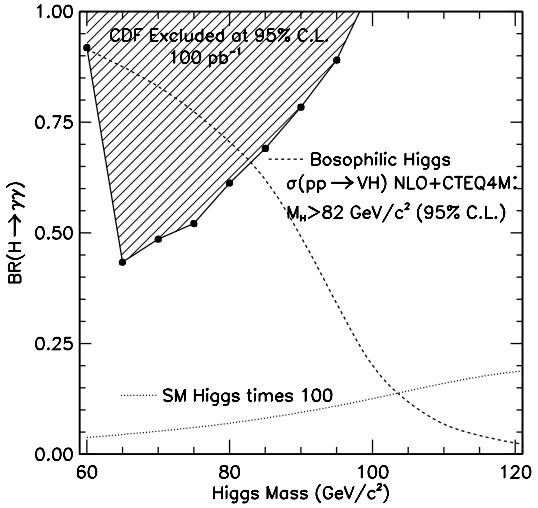

Figure 11: Upper limit at 95% C.L. on the branching ratio for $H \to \gamma\gamma$ assuming standard model production for $W/Z + H$ [13]. The dashed curve shows the branching fraction for a bosophilic $H \to \gamma\gamma$ from reference [5].

References

[1] E. Perazzi, G. Ridolfi, and F. Zwirner, hep-ph/0005076.

[2] L. Hall and C.Kolda, Phys. Lett. B **459**, 213 (1999);
K. Cheung, Phys. Rev. D **61**, 015005 (2000).

[3] T.G. Rizzo, Phys. Rev. D **51**, 1064 (1995).

[4] H. Haber, G. Kane, and T. Sterling, Nucl. Phys. **B161**, 493 (1979).

[5] A. Stange, W. Marciano, and S. Willenbrock, Phys. Rev. D **49**, 1354 (1994).

[6] M.A. Diaz and T.J. Weiler, hep-ph/9401259.

[7] A.G. Akeroyd, Phys. Lett. B **368**, 89 (1996).

[8] K. Lane, Phys. Lett. B **357**, 624 (1995).

[9] E. Cremmer, B. Julia, J. Scherck, S. Ferrara, L. Girardello, and P. van Nieuwenhuizen, Nucl. Phys. B **147**, 105 (1979).

[10] T. Bhattacharya and P. Roy, Phys. Rev. D **38**, 2284 (1988);
D.A. Dicus, S. Nandi, and J. Woodside, Phys. Rev. D **41**, 2347 (1990);
D.A. Dicus and P. Roy, Phys. Rev. D **42**, 938 (1990);
D.A. Dicus and S. Nandi, Phys. Rev. D **56**, 4166 (1997);

[11] E. Perazzi, G. Ridolfi, and F. Zwirner, hep-ph/0001025.

[12] DELPHI Collaboration, P. Abreu *et al.*, Phys. Lett. B **494**, 203 (2000).

[13] M. Smith and S. Willenbrock, private communication; T. Han and S. Willenbrock, Phys. Lett. B **273**, 167 (1991).

[14] M.C. Gonzalez-Garcia, S.M. Lietti, and S.F. Novaes, Phys. Rev. D **57**,7045 (1998).

[15] OPAL Collaboration, K. Ackerstaff *et al.*, Eur. Phys. J. **C 1**, 31 (1998).

[16] ALEPH Collaboration, R. Barate *et al.*, Phys. Lett. B **464**, 311 (1999).

[17] DO Collaboration, B. Abbott, *et al.*, Phys. Rev. Lett. **82** 2244 (1999).

[18] CDF Collaboration, F. Abe *et al.*, Phys. Rev. Lett. **70**, 2232 (1993).

[19] CDF Collaboration, F. Abe *et al.*, Phys. Rev. D **59**, 092002 (1999).

[20] CDF Collaboration, F. Abe *et al.*, Nucl. Instrum. Methods, A **271**, 387 (1988).

[21] The z (longitudinal) axis is along the proton beam axis; r is the transverse coordinate. Pseudorapidity (η) is $\eta \equiv -\ln(\tan(\theta/2))$, where θ is the polar angle. Transverse energy is defined as $E_T = E \sin\theta$.

[22] D. Amidei *et al.*, Nucl. Instrum. Methods, A **350**, 73 (1994).

[23] The trigger towers consist of two calorimeter towers in the central region, covering $0.1 \times 15^\circ$ in $\eta - \phi$ space. A typical CEM photon trigger cluster consists of 1 trigger tower, although neighboring trigger towers with more than 1 GeV can be added, as well as *their* neighbors.

[24] The cluster for a photon in the central electromagnetic calorimeter consists of one calorimeter tower of 0.1 in η times 15° in ϕ and the two calorimeter towers on either side in η, unless the tower is at one of the boundaries at $\eta = 0$ or $\eta = 1$, in which case the cluster is only two towers.

[25] CDF Collaboration, F. Abe *et al.*, Phys. Rev. Lett. **73**, 1662 (1994); Phys. Rev. **D 48**, 2998 (1993).

[26] T. Sjöstrand, Comput. Phys. Commun. **82**, 74 (1994); H. Bengtsson and T. Sjöstrand, Comput. Phys. Commun. **46**, 43 (1987). We use Version 6.1.

[27] CTEQ Collaboration, H. L. Lai *et al.*, Phys. Rev. D **55**, 1280 (1997). The 'L' distributions are used with LO calculations, and the 'M' distributions are used with NLO calculations.

[28] We consider "narrow" to mean widths comparable to or less than the mass resolution.

[29] CDF Collaboration, F. Abe *et al.*, Phys. Rev. D **56**, R1357 (1997).

[30] $\not\!\!E_T$ is defined to be the magnitude of the vector sum of transverse energy in all calorimeter towers with $|\eta| < 3.6$.

[31] CDF Collaboration, F. Abe *et al.*, Phys. Rev. D **50**, 2966 (1994); Phys. Rev. Lett. **73**, 2662 (1994).

[32] See CDF Collaboration, F. Abe *et al.*, Phys. Rev. D **45**, 1488 (1992) for a description of the jet-finding algorithm and the jet energy corrections.